BIOCHEMISTRY
including biophysical chemistry & molecular biology
Article

Biochemistry **2010,** *49,* 3477–3486 3477
DOI: 10.1021/bi100261c

Calcium-Induced Structural Transitions of the Calmodulin−Melittin System Studied by Electrospray Mass Spectrometry: Conformational Subpopulations and Metal-Unsaturated Intermediates[†]

Jingxi Pan and Lars Konermann*

Department of Chemistry, The University of Western Ontario, London, Ontario N6A 5B7, Canada

Received February 20, 2010; Revised Manuscript Received March 20, 2010

ABSTRACT: Calmodulin (CaM) is a calcium-sensing protein that can bind to and activate various target enzymes. Here, electrospray ionization mass spectrometry (ESI-MS) was used to investigate calcium-induced structural changes of CaM, as well as binding to the model target melittin (Mel). Nonspecific metalation artifacts were eliminated by conducting the experiments in negative ion mode and with calcium tartrate as metal source [Pan et al. (2009) *Anal. Chem. 81*, 5008]. Two coexisting CaM subpopulations can be distinguished on the basis of their ESI charge state distributions, namely, relatively disordered conformers (CaM_D, high charge states) and more tightly folded proteins (CaM_F, low charge states). Calcium titration experiments on isolated CaM reveal that the transition from apo-CaM_D to $Ca_4 \cdot CaM_F$ proceeds with apparent K_d values of 10, 14, 30, and 12 μM. In the presence of Mel, a gradual [Ca^{2+}] increase results in an overall population shift from apo-CaM_D to $Ca_4 \cdot CaM_F \cdot$Mel. This transition involves various intermediates, $Ca_n \cdot CaM_F \cdot$Mel with $n = 0, ..., 3$, as well as apo-$CaM_D \cdot$Mel. Thus, neither the binding of four Ca^{2+} nor the existence of a tightly folded CaM conformation is a prerequisite for target binding. Millisecond time-resolved ESI-MS experiments were conducted to monitor the response of a premixed CaM−Mel solution to a calcium concentration jump, thereby mimicking the conditions encountered in a cellular signaling context. The resulting data suggest that the formation of $Ca_4 \cdot CaM_F \cdot$Mel proceeds along three parallel kinetic pathways: (1) metal binding to CaM_D followed by formation of a compact protein−target complex, (2) folding of the apoprotein, then target binding, followed by metal complexation, (3) target binding to apo-CaM_D followed by sequential metal binding. The exact structural properties of the various metal-unsaturated CaM species, as well as their physiological roles, remain to be elucidated.

Intercellular communication involves the binding of effectors such as hormones or metal ions to specific protein receptors. Calmodulin (CaM)[1] is a highly conserved protein that is involved in numerous eukaryotic calcium signaling pathways (*1*, *2*). CaM has a bilobal architecture with distinct N-terminal and C-terminal domains. In the calcium-free (apo) form, each of these domains folds into a twisted four-helix bundle while retaining a high degree of internal dynamics (*3*). The N-terminal helices A/B and C/D, as well as the C-terminal helices E/F and G/H, form helix−turn−helix motifs that act as EF-hand calcium binding sites. The domains are connected by a flexible linker (*4*) (Figure 1).

External stimuli can trigger a sudden increase in the cytoplasmic Ca^{2+} concentration from 10^{-7} to ca. 10^{-5} M (*5*), and CaM binds these metal ions with micromolar affinity (*1*, *6*−*12*). The formation of calcium-saturated $Ca_4 \cdot$CaM leads to dramatic structural changes, involving helix reorientations and the exposure of hydrophobic elements in both domains (*3*, *4*). The crystal structure of $Ca_4 \cdot$CaM reveals a dumbbell-shaped conformation, where the N- and C-terminal lobes are separated by a long helical linker (*5*, *13*). However, in solution this linker is dynamic and only partially helical as shown by NMR spectroscopy (*1*, *3*−*5*).

In the presence of calcium CaM forms noncovalent complexes with target enzymes, resulting in target activation. Hundreds of different proteins can interact with CaM, including many phosphatases and kinases (*14*, *15*). Some insights into the mechanism of CaM-mediated target activation have been obtained on the basis of X-ray studies involving peptides that represent isolated target segments. These peptides share a basic and amphiphilic character, and they typically form an α-helix in their CaM-bound form (*1*, *15*−*17*). In the most commonly encountered ("canonical") binding mode CaM collapses into a compact, globular structure. In these complexes the central CaM linker forms a loop, allowing the two domains to engulf the target peptide and interact with it through hydrophobic and electrostatic interactions (*18*) (Figure 1). However, some targets interact with CaM in different ways, e.g., by binding to only one of the two lobes (*1*).

A number of studies have suggested that the presence of fully metalated $Ca_4 \cdot$CaM is a prerequisite for target binding and activation (*6*, *19*, *20*). Yet, the intracellular Ca^{2+} concentration rarely reaches levels that are capable of saturating all four EF-hands (*8*, *10*). It therefore appears unlikely that the formation of CaM−target complexes generally occurs via a simple two-stage mechanism where complexation of four metal ions is followed by target

[†]This work was supported by the Natural Sciences and Engineering Research Council of Canada (NSERC), the Canada Foundation for Innovation (CFI), and the Canada Research Chairs Program.

*To whom correspondence should be addressed. Telephone: (519) 661-2111 ext 86313. Fax: (519) 661-3022. E-mail: konerman@uwo.ca.

[1]Abbreviations: CaM, calmodulin; CaM·Mel, noncovalent complex of calmodulin and melittin; CaM_D, disordered calmodulin conformer; CaM_F, folded calmodulin conformer; ESI-MS, electrospray ionization mass spectrometry; Mel, melittin; *n*, number of calcium ions bound to calmodulin; NMR, nuclear magnetic resonance.

Published on Web 03/22/2010

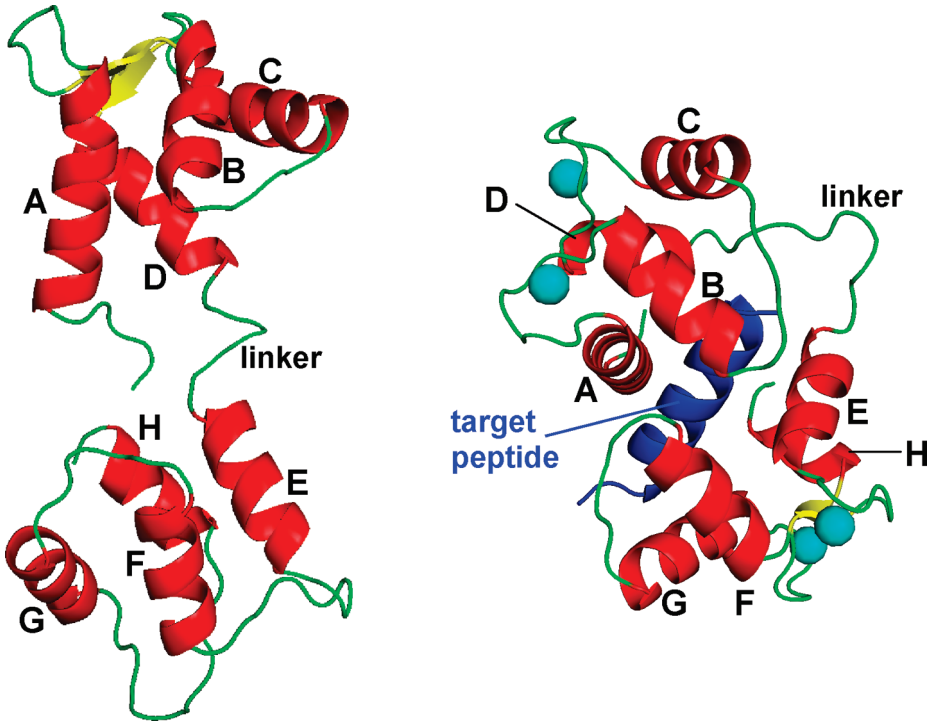

FIGURE 1: Three-dimensional structure of apo-CaM (PDB code 1CFD (*3*), left) and an example of a canonical $Ca_4 \cdot CaM \cdot$target complex (PDB code 1CM1 (*18*), right). CaM helices A−H are shown in red, and the target peptide is depicted in dark blue. Cyan-colored spheres represent calcium ions.

binding. Alternative scenarios have been proposed that involve metal-unsaturated CaM−target complexes (*9*−*11*, *16*, *21*−*23*). A difficulty encountered in many previous studies is the low selectivity of traditional titration methods that rely on optical readouts or activity assays, leading to possible ambiguities in the determination of metalation levels.

A number of electrospray ionization mass spectrometry (ESI-MS) techniques have been developed in recent years that are capable of providing detailed information on various aspects of protein−ligand interactions. For example, the structure and dynamics of noncovalent complexes can be probed by using ESI-MS in combination with hydrogen exchange (*24*−*26*), chemical labeling (*17*, *27*), cross-linking (*28*), or ion mobility measurements (*29*). Conceptually the most straightforward avenue is a direct mass analysis after transfer of intact solution-phase complexes into the gas phase by ESI. These measurements allow the detection of coexisting binding states, as well as the determination of the corresponding stoichiometries. In several cases it has even been possible to measure K_d values based on the signal intensities of free vs bound gas-phase species (*30*−*33*). Factors that may have to be considered for such binding affinity studies include differences in response factors (*34*), the possible disruption of noncovalent bonds during or after ESI (*35*), and the potential occurrence of nonspecific binding events (*36*). These caveats notwithstanding, direct ESI-MS measurements have become an extremely useful tool for gaining insights into biomolecular interactions (*37*−*39*). In addition to providing information on protein binding events, this approach allows alterations in protein compactness to be monitored through changes in the ESI charge state distribution. Unfolded proteins generally form higher charge states [i.e., higher protonation (deprotonation) states in positive (negative) ion mode] than tightly folded conformers (*40*−*46*). In this way, ESI-MS can report simultaneously on inter- and intramolecular aspects of protein−ligand binding (*47*−*50*).

The direct ESI-MS approach has been applied to the calcium−CaM system in a number of studies (*10*, *16*, *51*−*59*). Measurements of this type tend to suffer from interferences caused by the tendency of metal ions to form nonspecific adducts, giving rise to gas-phase assemblies with elevated binding levels that do not exist in bulk solution (*60*−*62*). The use of negative ion ESI can help to mitigate this problem (*63*), but nonspecific metalation often persists even under those conditions. Several negative ion mode investigations reported that CaM binds up to four Ca^{2+} (*52*, *63*, *64*), which is consistent with the presence of four EF-hand metal binding sites (*1*). However, other negative ion studies found that the protein can accommodate up to eight calciums, a result that implies the occurrence of nonspecific adduction (*51*, *54*, *55*). Even higher calcium binding levels were observed in positive ion mode (*16*, *59*). Hence, considerable uncertainties remain regarding the number of calcium ions that are associated with CaM under a given set of conditions. Also, the exact relationships between metal binding, CaM conformational changes, and CaM−target interactions remain to be elucidated.

Our group recently demonstrated that the performance of calcium tartrate (Ca^{2+} $^{-}OOC-CH(OH)-CH(OH)-COO^{-}$) as metal source in ESI-MS-based Ca^{2+} binding studies is greatly superior to the widely used calcium chloride and acetate. Calcium tartrate results in almost complete elimination of nonspecific Ca^{2+} adduction in negative ion mode, while retaining preexisting solution-phase interactions (*65*). Tartrate is a weak calcium chelator ($K_d \approx 10^{-2}$ M) (*66*). Its mode of action likely involves the sequestration of metal ions during the final stages of droplet evaporation (*67*), thereby reducing the number of free Ca^{2+} that would otherwise undergo nonspecific ion pairing with protein carboxylates (*65*). Using calcium tartrate, this work examines the behavior of CaM in ESI-MS-based metal titration experiments. We then discuss titration data obtained in the presence of melittin (Mel), a peptide that represents a common model for studying

CaM−target interactions (*17*, *20*, *51*, *68*−*70*). Ultimately, time-resolved ESI-MS (*71*) is used for exploring the response of CaM to a sudden jump in calcium concentration. Compared to equilibrium titration experiments, these kinetic measurements more closely mimic the situation experienced by CaM in a cellular signaling context.

EXPERIMENTAL PROCEDURES

Materials. CaM was expressed and purified as described elsewhere (*72*). The protein used represents the chicken, bovine, and human variants, all of which share the same 148-residue primary structure (*73*) with a MW of 16706 Da and a calculated p*I* of 4.1 (*13*). N-Acetylation was not observed for the samples used here (*68*). Stock solutions of CaM were extensively dialyzed against 10 mM ammonium acetate before use. Mel (GIGAVLKVLTTGLPALISWIKRKRQQ-NH_2, MW = 2846.5 Da, p*I* = 12) (*68*) and calcium tartrate [(+)-L-(2*R*,3*R*) stereoisomer] were purchased from Sigma and used without further purification. Calcium tartrate was used as the calcium source for all experiments. All solutions used for ESI-MS contained 2 mM ammonium acetate at pH 7 and had a final CaM concentration of 10 μM.

Mass Spectrometry. ESI mass spectra were acquired on an Ultima API (Waters/Micromass, Manchester, U.K.) quadrupole time-of-flight (Q-TOF) instrument, utilizing a standard Z-spray ESI source in negative ion mode with a capillary voltage of 2 kV, cone voltage of 45 V, and RF lens 1 voltage of 40 V. The desolvation and source temperatures were set to 120 and 80 °C, respectively. N_2 was used as nebulizer and desolvation gas. Samples for equilibrium measurements were infused into the mass spectrometer at a flow rate of 10 μL min^{-1} via a syringe pump (Harvard Apparatus, South Natick, MA).

Details of the continuous-flow apparatus used for time-resolved ESI-MS measurements have been described elsewhere (*74*). Briefly, two syringes (termed 1 and 2) were connected to a concentric capillary mixing setup that was directly interfaced to a customized ESI source. Mixing of solutions from syringe 1 (40 μM CaM and 40 μM Mel in 2 mM NH_4Ac, 5 μL/min) and syringe 2 (80 μM calcium tartrate in 2 mM NH_4Ac, 15 μL/min) resulted in a Ca^{2+} concentration jump from 0 to 60 μM, with final CaM and Mel concentrations of 10 μM. The reaction time is determined by the distance between the mixing point and the ESI source. Efficient mixing of the setup has been demonstrated previously (*75*) and was confirmed for the experiments conducted here using pulsed hydrogen exchange control experiments on a bradykinin test system (data not shown). The mass spectrometer was calibrated with CsI in positive ion mode. Measured protein mass spectra were converted to mass distributions using the MassLynx MaxEnt deconvolution software provided by the instrument manufacturer. Binding of calcium (40 Da) induces a mass shift of 38 Da because metalation is accompanied by the loss of two protons (*63*). Theoretical calcium binding distributions were calculated using Maple (MapleSoft, Waterloo, Ontario, Canada), following a procedure similar to that outlined by Nemirovskiy et al. (*7*).

RESULTS AND DISCUSSION

Calcium Titration of CaM. Prior to studying metal binding to CaM in the presence of a target peptide, it is instructive to examine the behavior of the isolated protein. ESI mass spectra of CaM were acquired as a function of Ca^{2+} concentration. As expected, data recorded in the absence of externally added calcium (Figure 2A) are dominated by apo-CaM. The lack of metal

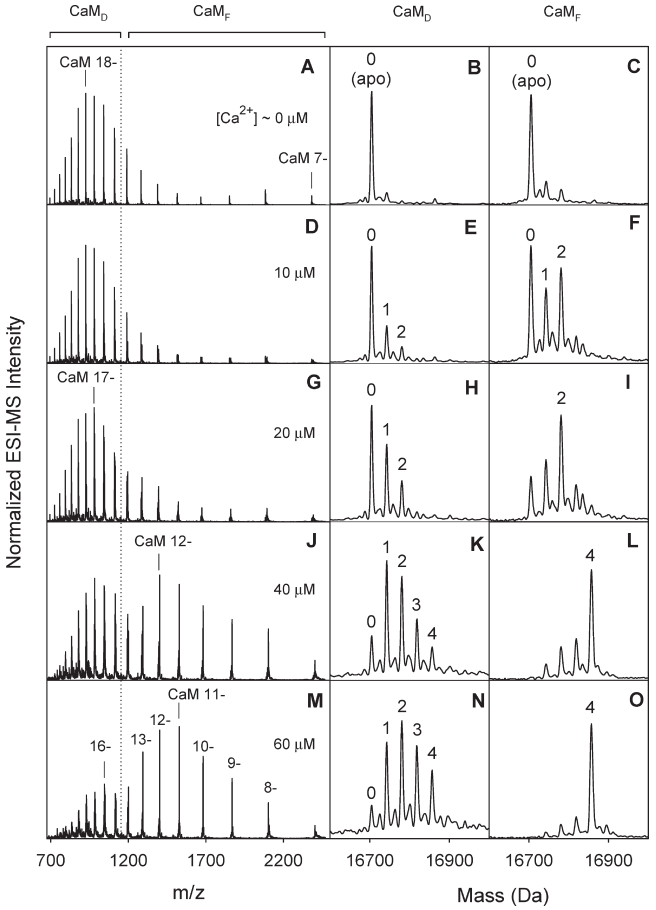

FIGURE 2: ESI mass spectra of 10 μM CaM recorded in negative ion mode after addition of calcium tartrate at different concentrations: 0 μM (A−C), 10 μM (D−F), 20 μM (G−I), 40 μM (J−L), and 60 μM (M−O). Panels on the left represent the raw data; selected CaM charge states are indicated as 8−, 9−, etc. Panels in the center column are deconvoluted mass distributions for high charge states (23− to 15−). Panels on the right are deconvoluted mass distributions for low charge states (14− to 7−). In the spectra on the left, the dotted vertical line separates high charge states (CaM_D, disordered protein) and low charge states (CaM_F, folded protein). The number of calcium ions corresponding to the individual peaks is denoted as 4, 3, 2, 1, and apo (corresponding to zero).

binding to the overwhelming majority of protein ions is evident from the deconvoluted mass distributions shown in Figure 2B,C. Low intensity signals for Ca·CaM and Ca_2·CaM reveal the presence of a very small amount of residual Ca^{2+} in the dialyzed samples. Apo-CaM shows a broad distribution of charge states with a maximum around 18− (Figure 2A). The predominance of highly charged protein ions indicates that most polypeptide chains adopt partially unfolded conformations in solution (*40*−*50*). This interpretation is consistent with NMR data that found apo-CaM to be semidisordered, particularly in the metal binding loops of the N-terminal domain, the central linker, and the entire C-terminal domain (*3*). In addition, Figure 2A shows less abundant protein ions in lower charge states, down to 7−. These signals are attributed to coexisting apo-CaM conformers that are more tightly folded. Using a global structural categorization, we can therefore distinguish ions representing relatively disordered solution-phase proteins (denoted as CaM_D) from signals that represent more compact conformations (referred to as CaM_F). In this notation the subscripts "D" and "F" stand for "disordered" and "folded", respectively. An approximate dividing line that separates the two subpopulations is indicated in Figure 2.

After addition of 60 μM Ca^{2+} the protein displays metal binding states n = 0, ..., 4 (Figure 2M−O). Importantly, the almost complete lack of signals with $n > 4$ confirms that nonspecific metalation artifacts are negligible due to the use of calcium tartrate in combination with negative ion mode (*65*). Hence, the ESI-MS data obtained here closely reflect the calcium binding behavior in solution, and the metalation states of CaM_D and CaM_F can be monitored separately.

The mass spectrum in Figure 2M for 60 μM $Ca^{2+}$is dominated by $Ca_4 \cdot CaM_F$ in a charge state distribution that is centered around 11−. The prevalence of relatively compact solution-phase conformers under these conditions is in accord with previous hydrogen exchange (*12*) and NMR studies (*4*). Yet, Figure 2M also reveals that a significant fraction of CaM_D is retained. The latter exist in metalation states from apo-CaM_D to $Ca_4 \cdot CaM_D$ (Figure 2N), and they have their most intense charge state at 16− (Figure 2M).

Readers are reminded that there is no general correlation between the net charge of a protein in solution and the charge states seen in ESI-MS (*76*, *77*). Instead, the solution-phase *structure* represents the main determinant of the ESI charge state distribution, as outlined in the introduction (*40*−*50*). Hence, it would be incorrect to attribute the less negative ions seen for $Ca_4 \cdot CaM_F$ to a trivial charge neutralization caused by the binding of positively charged metal ions. The inadequacy of such scenario is evident from the fact that even CaM_D in charge states up to at least 20− can carry four calciums (Figure 2M,N).

Figure 2 also includes data recorded at intermediate calcium concentrations of 10 μM (panels D−F), 20 μM (panels G−I), and 40 μM (panels J−L). The average metalation of both CaM_D and CaM_F increases with increasing calcium concentration. Close inspection reveals that this gradual change in metal binding is associated with a continuous shift in the maximum of the CaM_D charge state distribution, from 18− to 16− (Figure 2A,G, M). This phenomenon indicates a gradual conformational trend toward somewhat less disordered structures within the CaM_D subpopulation as more Ca^{2+} is added.

In addition to a dramatically higher metalation level for CaM_F than for CaM_D, the spectra in Figure 2 also reveal mechanistic differences in calcium binding for the two subpopulations. Some previous experiments suggested that metalation of individual EF-hands in CaM corresponds to independent events (*78*). Other studies favor models where each pair of EF-hands shows positive cooperativity, such that binding of one metal ion enhances the affinity for the other one (*4*, *5*, *52*). Interestingly, the data in Figure 2 reveal elements of both scenarios. The CaM_D metalation levels n = 0, ..., 4 in Figure 2E,H,K,N resemble binomial distributions that are consistent with four independent sites of similar affinity (*52*, *79*). In contrast, binding of the first two calcium ions to CaM_F is clearly cooperative. This is evident from the nonbinomial distribution in Figure 2F that has dominant peaks for n = 0 and n = 2 and a weaker signal for n = 1 (*52*). The metal affinity of the C-terminal lobe is believed to be higher than that of the N-terminal domain (*1*, *4*, *9*, *80*). Hence, the cooperativity seen in Figure 2F likely reflects the behavior of EF3 and EF4 in the C-terminal segment. The mass distributions in Figure 2 do not support the occurrence of cooperativity for the n = 3, 4 (EF1 and EF2) metalation steps of CaM_F, even when considering data for additional calcium concentrations that are not included in Figure 2 (not shown).

Summarizing the conclusions reached so far, an ESI-MS titration of CaM with Ca^{2+} reveals the presence of coexisting CaM conformers that can be roughly grouped into two categories according to their overall compactness, CaM_D and CaM_F. The validity of this grouping is supported by dramatic differences in calcium binding behavior for the two species. Members of both subpopulations can exist in metalation states n = 0 to n = 4. However, CaM_F has a significantly higher calcium affinity than CaM_D, such that $Ca_4 \cdot CaM_F$ becomes the dominant species at high calcium concentration. Metalation of the C-terminal lobe is cooperative only for CaM_F, not for CaM_D. N-Terminal binding of the third and fourth metal ion appears to be noncooperative for both conformers.

Table 1: Apparent Calcium−CaM Dissociation Constants (μM) Determined in Different Studies[a]

K_{d1}	K_{d2}	K_{d3}	K_{d4}	ref
7.7	2.7	31	31	*6*, *7*
33	0.7	25	0.4	*8*, *9*
~0.2	~0.2	~2	~2	*1*
7.9	1.7	35	8.9	*10*
33	0.5	158	10	*11*
n/d[b]	n/d[b]	14	9	*12*
10	14	30	12	this work

[a] K_{d1}−K_{d4} refer to four sequential metal binding equilibria in order of their occupancy; e.g., K_{d1} is for binding of the first calcium, etc. [b] Value not determined.

Apparent Dissociation Constants. The interaction of CaM with calcium is commonly discussed on the basis of a four-step binding/dissociation model: apo-CaM + calcium ↔ $Ca_1 \cdot CaM$; $Ca_1 \cdot CaM$ + calcium ↔ $Ca_2 \cdot CaM$; $Ca_2 \cdot CaM$ + calcium ↔ $Ca_3 \cdot CaM$; and $Ca_3 \cdot CaM$ + calcium ↔ $Ca_4 \cdot CaM$. Apparent K_d values for each step have been measured by different laboratories, yielding quite a range of results (Table 1) (*1*, *6*−*12*). Those earlier studies generally focused on the ensemble-averaged behavior, not taking into account the presence of coexisting CaM subpopulations that are clearly apparent from Figure 2. For comparing those previous findings to the data obtained here, we generated deconvoluted mass distributions from the *entire* mass spectra (Figure 2A,D, etc.), thereby considering the contributions of both CaM_D and CaM_F (Figure 3). Some features of the binding behavior become distorted by taking such an ensemble-averaged approach. For example, the n = 1, 2 cooperativity seen for CaM_F (Figure 2F) is no longer evident in Figure 3B. Conversely, the seemingly cooperative n = 3, 4 behavior (*52*) in Figure 3E is a superposition artifact that is not substantiated by inspection of the individual CaM_D and CaM_F data of Figure 2K,L. When modeling the combined mass distributions of Figure 3 within the four-step sequential scheme, it is found that the calcium binding behavior can be reasonably well described by four apparent K_d values of 10, 14, 30, and 12 μM (black circles in Figure 3). K_{d1}, K_{d3}, and K_{d4} are within the range of previously reported dissociation constants, whereas K_{d2} is somewhat larger than the literature values (Table 1). We note, however, that differences of this magnitude are not uncommon when measuring protein−ligand binding affinities by different assays (*12*, *25*), a notion that is supported by the wide spread of previously reported values in Table 1.

It would be interesting to apply K_d analyses of the type conducted in Figure 3 to CaM_D and CaM_F independently. Unfortunately, such a procedure is not feasible due to the unknown relative ESI-MS response factors of the two conformers. Existing methods for estimating response factors are not

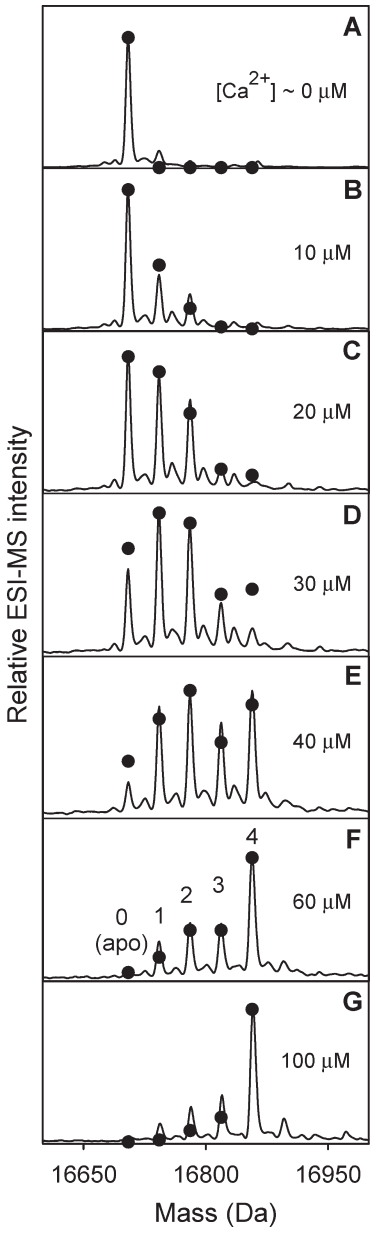

FIGURE 3: Deconvoluted ESI mass distributions of 10 μM CaM in the presence of calcium tartrate at different concentrations (0−100 μM, as indicated in each panel). The data shown here were obtained by including all charge states (23− to 7−) in the deconvolution procedure. Filled circles represent the abundance of the various calcium binding states, apo (0) to 4, calculated for a sequential binding model with four apparent K_d values (see text).

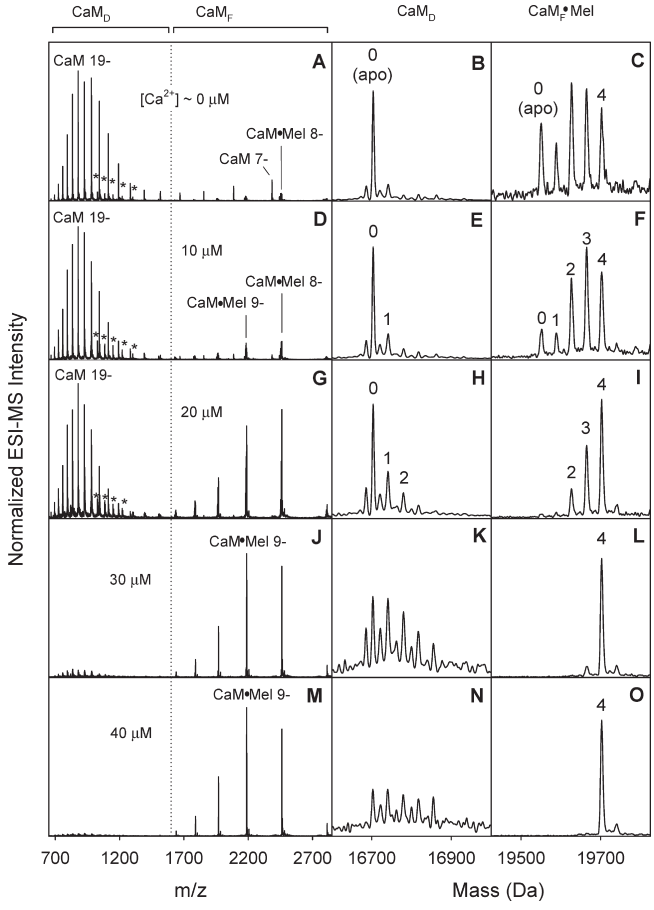

FIGURE 4: ESI mass spectra of 10 μM CaM in the presence of 10 μM Mel recorded after addition of calcium tartrate at different concentrations: 0 μM (A−C), 10 μM (D−F), 20 μM (G−I), 30 μM (J−L), and 40 μM (M−O). Panels in the center of the figure show mass distributions of CaM_D, obtained by deconvolution of the experimental data for $m/z < 1600$. Panels on the right depict mass distributions of $CaM_F \cdot$ Mel, resulting from deconvolution of the data for $m/z > 1600$. Asterisks in panels A, D, and G indicate signals in the high charge state range arising from apo-CaM · Mel complexes.

applicable to a highly heterogeneous system such as $Ca_n \cdot CaM_{D/F}$ (*34*, *81*). Compact protein conformers generally tend to have a lower response factor (*81*), and therefore the mass spectra of Figure 2 likely underrepresent the solution-phase contribution of CaM_F. Such a scenario could account for the relatively large value of K_{d2} in Table 1. Differences in the response factors of CaM_D and CaM_F will also affect the deconvoluted mass distributions of Figure 3 (*55*). Nonetheless, it is gratifying to see that the semiquantitative approach taken here provides estimates that are in reasonable agreement with previous conformer-averaged data.

Calcium Titration of the CaM−Melittin System. Melittin (Mel) is a 26-residue peptide found in bee venom. Exposure of CaM to Mel under saturating calcium conditions results in the formation of a $Ca_4 \cdot CaM \cdot$ Mel complex that has a peptide binding affinity on the order of 3 nM (*20*). Although the exact structure of this assembly remains unknown, it represents a widely used model system for exploring CaM−target interactions (*51*, *55*). Insights into the architecture of $Ca_4 \cdot CaM \cdot$ Mel come from small-angle X-ray scattering (*69*), various spectroscopic techniques (*20*), calorimetry (*70*), covalent labeling (*17*), and cross-linking studies (*68*, *82*). Accordingly, the complex possesses a tightly folded globular conformation where the two lobes engulf the α-helical target and bind it through hydrophobic and Coulombic interactions, in a manner similar to other canonical CaM−target assemblies (*1*, *70*) (Figure 1).

ESI mass spectra were recorded at various Ca^{2+} concentrations for samples containing 10 μM CaM and 10 μM Mel (Figure 4). As for the data of Figure 2, high and low charge states are assigned to conformational subpopulations CaM_D and CaM_F, respectively. Addition of calcium induces dramatic changes, from spectra that are dominated by apo-CaM_D (Figure 4A,B) to data that almost exclusively show $Ca_4 \cdot CaM_F \cdot$ Mel (Figure 4M, O). The charge state distribution of $Ca_4 \cdot CaM_F \cdot$ Mel is quite narrow and centered around 9− (Figure 4J,M). A comparison with the distribution observed for $Ca_4 \cdot CaM_F$ in the absence of Mel (Figure 2M) indicates that the target-bound complex is

substantially more compact. The mass distributions of Figure 4 (e.g., panels H and I) show that the calcium affinity of $CaM_F \cdot Mel$ is greatly enhanced compared to that of free CaM_D, a finding that is consistent with data for other target peptides (*10*, *20*). Cooperativity for the interaction of $CaM_F \cdot Mel$ with calcium is apparent from the nonbinomial distributions of Figure 4C,F. Free Mel is not observed in Figure 4 due to its low ionization efficiency in negative ion mode.

The presence of a tightly folded CaM−target complex is thought to be a prerequisite for the activation of many proteins (*1*). One goal of this work was to explore the minimum number of bound calcium ions required for the formation of such a compact assembly. As expected, Figure 4 confirms that tightly folded $Ca_4 \cdot CaM_F \cdot Mel$ becomes the most strongly populated species at high calcium concentration (Figure 4M−O). Surprisingly, however, Figure 4 also reveals the presence of compact $Ca_n \cdot CaM_F \cdot Mel$ assemblies in other metalation levels, from calcium-free complexes up to $n = 3$ (panels C, F, and I). These metal-unsaturated species are readily apparent for Ca^{2+} concentrations around 10 μM (Figure 4F), which is within the range typically encountered after Ca^{2+} influx into the cell (*1*, *5*). On the basis of their ESI charge states, the overall compactness of these unsaturated $CaM_F \cdot Mel$ complexes is indistinguishable from that of the canonical $Ca_4 \cdot CaM_F \cdot Mel$ structure. The observation of apo-$CaM_F \cdot Mel$ is particularly interesting, because it suggests the possible calcium-independent formation of a canonically bound complex. Figure 4 also demonstrates the presence of another type of assembly that is mostly calcium-free (marked by asterisks in panels A, D, and G; see also Figure 5A). The high charge states of this species (around 18−) attest to a disordered structure, such that it can be categorized as apo-$CaM_D \cdot Mel$.

Previous evidence for the occurrence of weak calcium-independent CaM · Mel complexation comes from equilibrium dialysis experiments (*20*). Unexpectedly, that earlier work suggested the presence of Mel:apo-CaM binding stoichiometries of 2:1 and higher, a scenario that is not confirmed by our observations. A previous positive ion ESI-MS study observed 1:1 binding of calcium-free CaM to a synthetic peptide (*16*). To the best of our knowledge, however, the current work provides the first evidence for the coexistence of apo-CaM · target complexes in two vastly different structures, apo-$CaM_D \cdot Mel$ and apo-$CaM_F \cdot Mel$. The latter exhibits a compact (possibly canonical) fold. The former may represent a structure where Mel is bound to just a single CaM lobe, allowing the other lobe and the central linker to remain extensively disordered. Some support for the feasibility of such a scenario comes from recent X-ray data for complexes involving noncanonical CaM targets (*1*).

Time Dependence of $Ca_4 \cdot CaM_F \cdot Mel$ Formation. The titration experiments of Figure 4 monitor CaM−target interactions as a function of calcium concentration. Such equilibrium studies provide interesting information, but they are not representative of the situation encountered by CaM in a cellular signaling context where the protein is premixed with its target(s) and experiences a sudden calcium influx. This concentration change occurs within micro- to milliseconds (*83*, *84*). Surprisingly, investigations into the kinetic mechanisms of CaM−metal and CaM−target interactions are rare (*11*).

Time-resolved ESI-MS allows the acquisition of mass spectra at various times after triggering a kinetic process by mixing of two solutions. The experiments involve the use of a customized ESI source that is coupled online to a continuous-flow mixing device (*71*). Using this approach, changes in the mass spectrum of a premixed solution containing CaM and Mel (10 μM each) were monitored following a $[Ca^{2+}]$ jump from ~0 to 60 μM (Figure 6). The high solution flow rate used in these experiments compromises the signal-to-noise ratio somewhat, but various species are nonetheless clearly discernible in the spectra. Small differences in the maxima of the charge state distributions compared to Figure 4 are attributed to the altered desolvation characteristics of the customized ESI source (*85*).

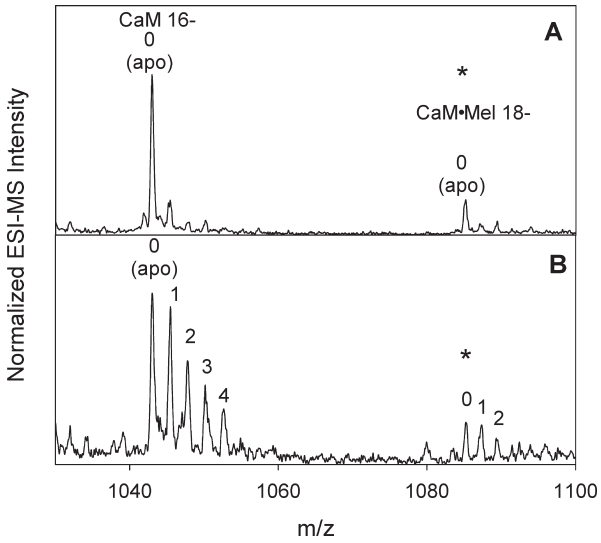

FIGURE 5: (A) Expanded view of the ESI mass spectrum in Figure 4D, obtained after equilibration of a solution containing CaM, Mel, and calcium tartrate (10 μM each). (B) Expanded view of the time-resolved spectrum in Figure 6A, obtained 40 ms after exposing a premixed solution containing CaM and Mel (10 μM each) to 60 μM calcium tartrate (final concentrations). Asterisks are meant to facilitate the identification of correspondingly marked signals in Figures 4 and 6.

The earliest time point that could be studied with our device represents a reaction time of 40 ms (Figure 6A). The resulting spectrum is dominated by CaM_D in various metalation states. The most intense peaks correspond to apo-CaM_D, whereas the $n = 1, ..., 4$ species exhibit successively lower intensities (Figure 6B). This pattern remains roughly constant throughout the entire reaction, indicating that apo-CaM_D and the various $Ca_n \cdot CaM_D$ states are in rapid equilibrium with each other (Figure 6E,H) (*74*). After 30 s the abundance of CaM_D has reached a level close to zero (Figure 6J,K).

The depletion of CaM_D occurs concomitantly with the formation of $Ca_n \cdot CaM_F \cdot Mel$ (Figure 6J−L). The metalation pattern of the latter exhibits an interesting time dependence. Data obtained at 40 ms exhibit a distinct signal at $n = 2$, a more intense contribution for $n = 3$, and a dominant peak at $n = 4$ (Figure 6C). With increasing time there is a gradual change, where the $n = 2$ and subsequently the $n = 3$ peaks fade from the spectrum (Figure 6F,I) until ultimately only $Ca_4 \cdot CaM_F \cdot Mel$ is observable (Figure 6J,L). This behavior is consistent with sequential binding of the third and fourth calcium ion.

Comparison of Figure 6 with the corresponding equilibrium data (Figure 4A, D) reveals a lack of apo-CaM_F in the kinetic spectra. In contrast, $CaM_D \cdot Mel$ signals are observed in the high charge state region of both data sets (marked with asterisks in Figure 6A,D). Close inspection reveals that under kinetic conditions these species are mostly in the apo state, in addition to $n = 1$, 2 metalation (Figure 5B).

Kinetic Model for $Ca_4 \cdot CaM_F \cdot Mel$ Formation. Time-resolved ESI-MS reveals a surprisingly complex picture of the

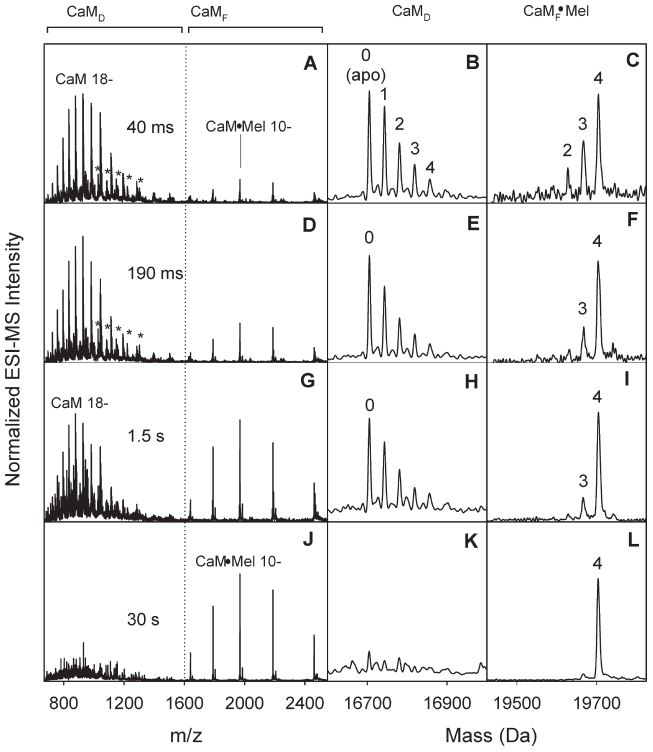

FIGURE 6: ESI mass spectra recorded at various time points after exposing a premixed solution containing CaM and Mel (10 μM each) to 60 μM calcium tartrate (final concentrations): (A) 40 ms, (B) 190 ms, (C) 1.5 s, and (D) 30 s. Further information is provided in the captions of Figures 1 and 3.

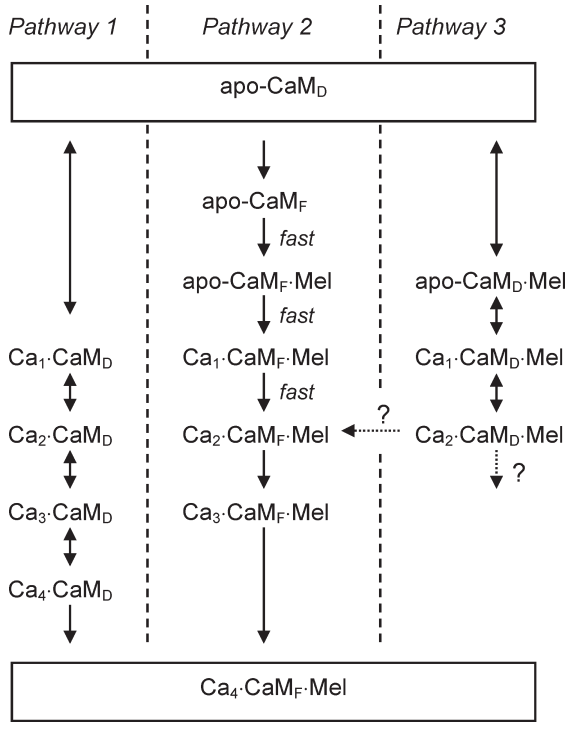

FIGURE 7: Proposed kinetic mechanism for the formation of Ca_4·CaM_F·Mel from apo-CaM_D under the conditions of Figure 6. The scheme involves three parallel pathways. Reaction steps that are essentially irreversible are indicated as single-headed arrows; rapid equilibration is denoted by double-headed arrows. Dashed arrows with question marks denote steps for which insufficient information is available. Further information is provided in the text.

Ca_4·CaM_F·Mel formation process from apo-CaM_D, involving coexisting conformers in various metalation states, and a mix of target-bound and target-free protein species. The current section collates this information into a kinetic model. The proposed mechanism involves three parallel pathways, each of which is represented by a vertical progression in Figure 7.

Pathway 1 reflects the occurrence of rapid equilibration between apo-CaM_D and Ca_n·CaM_D with n = 1, ..., 4 (Figure 6B,E, H). These equilibration processes are represented by double-headed arrows in Figure 7. Target binding and folding to the canonical Ca_4·CaM_F·Mel structure can occur once the Ca_4·CaM_D state has been reached. This final step is indicated by a unidirectional arrow. On the basis of our data it cannot be decided whether CaM folding and Mel binding occur concomitantly or whether one precedes the other during this terminal transition on pathway 1.

Pathway 2 accounts for the presence of various Ca_n·CaM_F·Mel assemblies throughout the reaction (Figure 6C,F,I,L). As a general fact, any transiently formed species will be undetectable if its decay rate greatly exceeds the rate of formation (*86*). Pathway 2 represents such a scenario where not all of the kinetic species are observable in the time-resolved data of Figure 6. Importantly, however, the existence of all species can be verified under equilibrium conditions (Figure 4). Pathway 2 begins with formation of apo-CaM_F. Successive target binding and the association with two Ca^{2+} occur rapidly. The first kinetic intermediate that accumulates on this pathway is Ca_2·CaM_F·Mel (Figure 6C). Subsequent binding of two additional Ca^{2+} results in formation of the Ca_4·CaM_F·Mel reaction product.

The detection of apo-CaM_D·Mel and Ca_n·CaM_D·Mel (n = 1, 2; asterisks in Figures 5B and 6A,D) suggests the existence of a third pathway that commences by association of Mel with apo-CaM_D, followed by binding of a first and then a second calcium ion. As mentioned earlier, the intermediates formed in this way may have Mel bound to only a single CaM lobe, in a fashion similar to that seen for some noncanonical targets (*1*). Unfortunately, Figure 6 does not provide information on the kinetic fate of these species. A transition to a compact CaM conformation could result in merging of pathways 3 and 2. Alternatively, Ca_2·CaM_D·Mel could bind two more calcium ions before undergoing a final transition to Ca_4·CaM_F·Mel. These two possibilities are indicated by dotted arrows in Figure 7.

Because the rate constants associated with our model remain unknown, it is not possible to predict the fluxes through the individual reaction pathways. Notably, rate constants may not be the only determinant of kinetic partitioning because preexisting inhomogeneities within the apo-CaM_D pool might favor one pathway over another. For example, non-native cis/trans isomerization of the protein's two X−Pro bonds would likely interfere with the initial folding step (apo-CaM_D → apo-CaM_F) on pathway 2 (*87*). Kinetic experiments can never provide ultimate proof of a reaction mechanism, but they allow the development of models that are compatible with the measured data. Hence, the parallel pathway mechanism of Figure 7 is a possible scenario that captures the major features of our time-resolved data, but other models could exist as well.

CONCLUSIONS

This work employed ESI-MS for gaining insights into the interaction of CaM with Ca^{2+} and a model target peptide, Mel. The use of calcium tartrate ensured that the metal binding distributions observed in the gas phase closely resemble those in solution. Using the ESI charge state distribution as a probe for

the protein compactness in solution, we found a surprisingly high degree of conformational heterogeneity. Under most conditions studied, CaM forms coexisting conformers. Using a global categorization, one can distinguish disordered species (CaM_D) from proteins that adopt more folded structures (CaM_F). Both conformational ensembles appear in a wide range of metal binding states, from the apoprotein all the way to $Ca_4 \cdot CaM$. The majority of these species are capable of target binding, evident from the direct observation of various $Ca_n \cdot CaM_{D/F} \cdot Mel$ complexes in the mass spectra. The only two species that were unobservable correspond to the disordered conformers $Ca_3 \cdot CaM_D \cdot Mel$ and $Ca_4 \cdot CaM_D \cdot Mel$, suggesting that these assemblies are highly unstable and, once formed, would likely undergo rapid turnover to the corresponding folded conformers.

Our work confirms an overall trend toward the formation of tightly folded $Ca_4 \cdot CaM_F \cdot Mel$ in the presence of elevated calcium levels, as expected on the basis of previous structural and biochemical evidence (*1*). Yet, neither the binding of four calcium ions nor the presence of a tightly folded CaM conformation is a prerequisite for the formation of a CaM−target complex. To a certain extent, the kinetic experiments conducted here mimic the physiological situation where CaM and target molecules are premixed in the cytoplasm prior to experiencing a sudden increase in calcium concentration. The kinetic transition from apo-CaM_D to $Ca_4 \cdot CaM_F \cdot Mel$ involves a number of transient intermediates. We propose that the reaction occurs along three parallel pathways (Figure 7): metal binding to CaM_D followed by formation of a compact protein−target complex (pathway 1), folding of the apoprotein, then target binding, followed by sequential metal complexation (pathway 2), and target binding to apo-CaM_D followed by metal binding (pathway 3). These reactions occur on a time scale of 30 s under the conditions of this work, which is surprisingly slow when considering the physiological role of CaM as a signal-transducing molecule. However, it is possible that the kinetics are accelerated in the crowded environment of the cytoplasm (*88*).

The observation of metal-unsaturated $CaM \cdot Mel$ complexes in this work is consistent with earlier reports that substoichiometric amounts of calcium can be sufficient for CaM-mediated target activation (*9*−*11*, *16*, *21*−*23*). Models where complexation of four calcium ions by CaM is a prerequisite for target binding (*6*, *19*, *20*) can be ruled out. Instead, our results support a different view of the CaM regulatory mechanism whereby target binding can already occur under conditions where not all of the EF-hands are occupied and where subsequent metal binding after calcium influx is required for full activation of the target (*23*). It remains an open question which of the assemblies observed here exhibit a conformation that corresponds to such a "fully activated" complex. On the basis of the ESI-MS data presented here there is no evidence for structural differences between the canonical $Ca_4 \cdot CaM_F \cdot Mel$ assembly and metal-unsaturated $Ca_n \cdot CaM_F \cdot Mel$ species with $n = 0$, ..., 3. However, ESI charge state distributions only provide a global view of protein structure. In future work, it will be interesting to use complementary approaches such as hydrogen/deuterium exchange or covalent labeling techniques (*41*) for gaining additional insights into the properties of these metal-unsaturated species. Considering the well-established role of Ca^{2+} as a chemical messenger, those future studies will likely uncover subtle but functionally important differences between metal-unsaturated and saturated CaM−target complexes.

ACKNOWLEDGMENT

We thank Drs. Kun Xu and Xiaoda Yang (Peking University) for expression and purification of the calmodulin samples used in this work.

REFERENCES

1. Vetter, S. W., and Leclerc, E. (2003) Novel aspects of calmodulin target recognition and activation. *Eur. J. Biochem. 270*, 404–414.
2. Drakenberg, T., Finn, B., and Forsen, S. (2007) in Biological Inorganic Chemistry: Structure and Reactivity (Bertini, I., Gray, H. B., Stiefel, E. I., and Valentine, J. S., Eds.) pp 635−646, University Science Books, Sausalito, CA.
3. Kuboniwa, H., Tjandra, N., Grzesiek, S., Ren, H., Klee, C. B., and Bax, A. (1995) Solution structure of calcium-free calmodulin. *Nat. Struct. Biol. 2*, 768–776.
4. Zhang, M., Tanaka, T., and Ikura, M. (1995) Calcium-induced conformational transition revealed by the solution structure of apo calmodulin. *Nat. Struct. Biol. 2*, 758–767.
5. Chazin, W. J. (1995) Releasing the calcium trigger. *Nat. Struct. Biol. 2*, 707–710.
6. Gregori, L., Gillevet, P. M., Doan, P., and Chau, V. (1985) Mechanism of enzyme regulation by calmodulin and Ca^{2+}. *Curr. Top. Cell Regul. 27*, 447–454.
7. Nemirovskiy, O., Giblin, D. E., and Gross, M. L. (1999) Electrospray ionization mass spectrometry and hydrogen/deuterium exchange for probing the interaction of calmodulin with calcium. *J. Am. Soc. Mass Spectrom. 10*, 711–718.
8. Klee, C. B. (1988) in Calmodulin (Cohen, P., and Klee, C. B., Eds.) pp 35−56, Elsevier, New York.
9. Wintrode, P. L., and Privalov, P. L. (1997) Energetics of target peptide recognition by calmodulin: a calorimetric study. *J. Mol. Biol. 266*, 1050–1062.
10. Shifman, J. M., Choi, M. H., Mihalas, S., Mayo, S. L., and Kennedy, M. B. (2006) Ca^{2+}/calmodulin-dependent protein kinase II (CaMKII) is activated by calmodulin with two bound calciums. *Proc. Natl. Acad. Sci. U.S.A. 103*, 13968–13973.
11. Park, H. Y., Kim, S. A., Korlach, J., Rhoades, E., Kwok, L. W., Zipfel, W. R., Waxham, M. N., Webb, W. W., and Pollack, L. (2008) Conformational changes of calmodulin upon Ca^{2+} binding studied with a microfluidic mixer. *Proc. Natl. Acad. Sci. U.S.A. 105*, 542–547.
12. Zhu, M. M., Rempel, D. L., Zhao, J., Giblin, D. E., and Gross, M. L. (2003) Probing Ca^{2+}-induced conformational changes in porcine calmodulin by H/D exchange and ESI-MS: effect of cations and ionic strength. *Biochemistry 42*, 15388–15397.
13. Chattopadhyaya, R., Meador, W. E., Means, A. R., and Quiocho, F. A. (1992) Calmodulin structure refined at 1.7 Å resolution. *J. Mol. Biol. 228*, 1177–1192.
14. Crivici, A., and Ikura, M. (1995) Molecular and structural basis of target recognition by calmodulin. *Annu. Rev. Biophys. Biomol. Struct. 24*, 85–116.
15. Frederick, K. K., Marlow, M. S., Valentine, K. G., and Wand, A. J. (2007) Conformational entropy in molecular recognition by proteins. *Nature 448*, 325–330.
16. Hill, T. J., Lafitte, D., Wallace, J. I., Cooper, H. J., Tsvetkov, P. O., and Derrick, P. J. (2000) Calmodulin-peptide interactions: apocalmodulin binding to the myosin light chain kinase target site. *Biochemistry 39*, 7284–7290.
17. Wong, J. W. H., Maleknia, S. D., and Downard, K. M. (2005) Hydroxyl radical probe of the calmodulin-melittin complex interface by electrospray ionization mass spectrometry. *J. Am. Soc. Mass Spectrom. 16*, 225–233.
18. Wall, M. E., Clarage, J. B., and Phillips, G. N., Jr. (1997) Motions of calmodulin characterized using both Bragg and diffuse X-ray scattering. *Structure 5*, 1599–1612.
19. Huang, C. Y., Chau, V., Chock, P. B., Wang, J. H., and Sharma, R. K. (1981) Mechanism of activation of cyclic nucleotide phosphodiesterase: requirement of the binding of four Ca^{2+} to calmodulin for activation. *Proc. Natl. Acad. Sci. U.S.A. 78*, 871–874.
20. Maulet, Y., and Cox, J. A. (1983) Structural changes in melittin and calmodulin upon complex formation and their modulation by calcium. *Biochemistry 22*, 5680–5686.
21. DeMaria, C. D., Soong, T. W., Alseikhan, B. A., Alvania, R. S., and Yue, D. T. (2001) Calmodulin bifurcates the local Ca^{2+} signal that modulates P/Q-type Ca^{2+} channels. *Nature 411*, 484–489.
22. Gao, Z. H., Krebs, J., VanBerkum, M. F., Tang, W. J., Maune, J. F., Means, A. R., Stull, J. T., and Beckingham, K. (1993) Activation of

four enzymes by two series of calmodulin mutants with point mutations in individual Ca^{2+} binding sites. *J. Biol. Chem. 268*, 20096–20104.
23. Kincaid, R. L., and Vaughan, M. (1986) Direct comparison of Ca^{2+} requirements for calmodulin interaction with and activation of protein phosphatase. *Proc. Natl. Acad. Sci. U.S.A. 83*, 1193–1197.
24. Zhu, M. M., Rempel, D. L., Du, Z., and Gross, M. L. (2003) Quantification of protein-ligand interactions by mass spectrometry, titration, and H/D exchange: PLIMSTEX. *J. Am. Chem. Soc. 125*, 5252–5253.
25. Powell, K. D., Ghaemmaghami, S., Wang, M. Z., Ma, L., Oas, T. G., and Fitzgerald, M. C. (2002) A general mass spectrometry-based assay for the quantitation of protein-ligand binding interactions in solution. *J. Am. Chem. Soc. 124*, 10256–10257.
26. Pan, J., Han, J., Borchers, C. H., and Konermann, L. (2009) Hydrogen/deuterium exchange mass spectrometry with top-down electron capture dissociation for characterizing structural transitions of a 17 kDa protein. *J. Am. Chem. Soc. 131*, 12801–12808.
27. Mendoza, V. L., and Vachet, R. W. (2009) Probing protein structure by amino acid-specific covalent labeling and mass spectrometry. *Mass Spectrom. Rev. 28*, 785–815.
28. Sinz, A. (2003) Chemical cross-linking and mass spectrometry for mapping three-dimensional structures of proteins and protein complexes. *J. Mass Spectrom. 38*, 1225–1237.
29. Ruotolo, B. T., Giles, K., Campuzano, I., Sandercock, A. M., Bateman, R. H., and Robinson, C. V. (2005) Evidence for macromolecular protein rings in the absence of bulk water. *Science 310*, 1658–1661.
30. Jørgensen, T. J. D., Roepstorff, P., and Heck, A. J. R. (1998) Direct determination of solution binding constants for noncovalent complexes between bacterial cell wall peptide analogues and vancomycin group antibiotics by electrospray ionization mass spectrometry. *Anal. Chem. 70*, 4427–4432.
31. Wang, W., Kitova, E. N., and Klassen, J. S. (2003) Influence of solution and gas phase processes on protein-carbohydrate binding affinities determined by nanoelectrospray Fourier transform ion cyclotron resonance mass spectrometry. *Anal. Chem. 75*, 4945–4955.
32. Jecklin, M. C., Touboul, D., Bovet, C., Wortmann, A., and Zenobi, R. (2008) Which electrospray-based ionization method best reflects protein-ligand interactions found in solution? A comparison of ESI, nanoESI, and ESSI for the determination of dissociation constants with mass spectrometry. *J. Am. Soc. Mass Spectrom. 19*, 332–343.
33. Frycak, P., and Schug, K. A. (2007) On-line dynamic titration: determination of dissociation constants for noncovalent complexes using Gaussian concentration profiles by electrospray ionization mass spectrometry. *Anal. Chem. 79*, 5407–5413.
34. Gabelica, V., Rosu, F., and De Pauw, E. (2009) A simple method to determine electrospray response factors of noncovalent complexes. *Anal. Chem. 81*, 6708–6715.
35. Robinson, C. V., Chung, E. W., Kragelund, B. B., Knudsen, J., Aplin, R. T., Poulsen, F. M., and Dobson, C. M. (1996) Probing the nature of noncovalent interactions by mass spectrometry. A study of protein-CoA ligand binding and assembly. *J. Am. Chem. Soc. 118*, 8646–8653.
36. Wang, W., Kitova, E. N., and Klassen, J. S. (2005) Nonspecific protein-carbohydrate complexes produced by nanoelectrospray ionization. Factors influencing their formation and stability. *Anal. Chem. 77*, 3060–3071.
37. Loo, J. A. (2005) in The Encyclopedia of Mass Spectrometry (Gross, M. L., and Caprioli, R. M., Eds.) pp 289−299, Elsevier, Amsterdam.
38. Benesch, J. L. P., Ruotolo, B. T., Simmons, D. A., and Robinson, C. V. (2007) Protein complexes in the gas phase: technology for structural genomics and proteomics. *Chem. Rev. 107*, 3544–3567.
39. Heck, A. J. R. (2008) Native mass spectrometry: a bridge between interactomics and structural biology. *Nat. Methods 5*, 927–933.
40. Konermann, L. (2007) A minimalist model for exploring conformational effects on the electrospray charge state distribution of proteins. *J. Phys. Chem. B 111*, 6534–6543.
41. Kaltashov, I. A., and Eyles, S. J. (2005) Mass Spectrometry in Biophysics, John Wiley and Sons, Hoboken, NJ.
42. Sogbein, O. O., Simmons, D. A., and Konermann, L. (2000) The effects of pH on the kinetic reaction mechanism of myoglobin unfolding studied by time-resolved electrospray ionization mass spectrometry. *J. Am. Soc. Mass Spectrom. 11*, 312–319.
43. Grandori, R. (2002) Detecting equilibrium cytochrome *c* folding intermediates by electrospray ionization mass spectrometry: two partially folded forms populate the molten globule state. *Protein Sci. 11*, 453–458.
44. Borysic, A. J. H., Radford, S. E., and Ashcroft, A. E. (2004) Co-populated conformational ensembles of β2-microglobulin uncovered quantitatively by electrospray ionization mass spectrometry. *J. Biol. Chem. 279*, 27069–27077.
45. Cai, X., and Dass, C. (2003) Conformational analysis of proteins and peptides. *Curr. Org. Chem. 7*, 1841–8154.
46. Frimpong, A. K., Abzatimov, R. R., Uversky, V. N., and Kaltashov, I. A. (2010) Characterization of intrinsically disordered proteins with electrospray ionization mass spectrometry: conformational heterogeneity of alpha-synuclein. *Proteins 78*, 714–722.
47. Katta, V., and Chait, B. T. (1991) Observation of the heme-globin complex in native myoglobin by electrospray-ionisation mass spectrometry. *J. Am. Chem. Soc. 113*, 8534–8535.
48. Vis, H., Heinemann, U., Dobson, C. M., and Robinson, C. V. (1998) Detection of a monomeric intermediate associated with dimerization of protein Hu by mass spectrometry. *J. Am. Chem. Soc. 120*, 6427–6428.
49. Wilson, D. J., Rafferty, S. P., and Konermann, L. (2005) Kinetic unfolding mechanism of the inducible nitric oxide synthase oxygenase domain determined by time-resolved electrospray mass spectrometry. *Biochemistry 44*, 2276–2283.
50. Gumerov, D. R., Mason, A. B., and Kaltashov, I. A. (2003) Interlobe communication in human serum transferrin: metal binding and conformational dynamics investigated by electrospray ionization mass spectrometry. *Biochemistry 42*, 5421–5428.
51. Nemirovskiy, O. V., Ramanathan, R., and Gross, M. L. (1997) Investigation of calcium-induced, noncovalent association of calmodulin with melittin by electrospray ionization mass spectrometry. *J. Am. Soc. Mass Spectrom. 8*, 809–812.
52. Hu, P., and Loo, J. A. (1995) Determining calcium-binding stoichiometry and cooperativity of parvalbumin and calmodulin by mass spectrometry. *J. Mass Spectrom. 30*, 1076–1082.
53. Shirran, S. L., and Barran, P. E. (2009) The use of ESI-MS to probe the binding of divalent cations to calmodulin. *J. Am. Soc. Mass Spectrom. 20*, 1159–1171.
54. Pukala, T. L., Urathamakul, T., Watt, S. J., Beck, J. L., Jackway, R. J., and Bowie, J. H. (2008) Binding studies of nNOS-active amphibian peptides and Ca^{2+} calmodulin, using negative ion electrospray ionisation mass spectrometry. *Rapid Commun. Mass Spectrom. 22*, 3501–3509.
55. Mathur, S., Badertscher, M., Scott, M., and Zenobi, R. (2007) Critical evaluation of mass spectrometric measurement of dissociation constants: accuracy and cross-validation against surface plasmon resonance and circular dichroism for the calmodulin-melittin system. *Phys. Chem. Chem. Phys. 9*, 6187–6198.
56. Watt, S. J., Oakley, A., Sheil, M. M., and Beck, J. L. (2005) Comparison of negative and positive ion electrospray ionization mass spectra of calmodulin and its complex with trifluoperazine. *Rapid Commun. Mass Spectrom. 19*, 2123–2130.
57. Ly, T., and Julian, R. R. (2008) Protein-metal interactions of calmodulin and α-synuclein monitored by selective noncovalent adduct protein probing mass spectrometry. *J. Am. Soc. Mass Spectrom. 19*, 1663–1672.
58. Wyttenbach, T., Grabenauer, M., Thalassinos, K., Scrivens, J. H., and Bowers, M. T. (2010) The effect of calcium ions and peptide ligands on the relative stabilities of the calmodulin dumbbell and compact structures. *J. Phys. Chem. B 114*, 437–447.
59. Lafitte, D., Capony, J. P., Grassy, G., Haiech, J., and Calas, B. (1995) Analysis of ion binding sites of calmodulin by electrospray ionization mass spectrometry. *Biochemistry 34*, 13825–13832.
60. Verkerk, U. H., and Kebarle, P. (2005) Ion-ion and ion-molecule reactions at the surface of proteins produced by nanospray. Information on the number of acidic residues and control of the number of ionized acidic and basic residues. *J. Am. Soc. Mass Spectrom. 16*, 1325–1341.
61. Turner, K. B., Monti, S. A., and Fabris, D. (2008) Like polarity ion/ion reactions enable the investigation of specific metal interactions in nucleic acids and their noncovalent assemblies. *J. Am. Chem. Soc. 130*, 13353–13363.
62. Deng, L., Sun, N., Kitova, E. N., and Klassen, J. S. (2010) Direct quantification of protein-metal ion affinities by electrospray ionization mass spectrometry. *Anal. Chem. 82*, 2170–2174.
63. Hu, P., Ye, Q.-Z., and Loo, J. A. (1994) Calcium stoichiometry determination for calcium binding proteins by electrospray ionization mass spectrometry. *Anal. Chem. 66*, 4190–4194.
64. Watt, S. J., Oakley, A., Sheil, M. M., and Beck, J. L. (2006) Comparison of negative and positive ion electrospray ionization mass spectra of calmodulin and its complex with trifluoperazine. *Rapid Commun. Mass Spectrom. 19*, 2123–2130.
65. Pan, J., Xu, K., Yang, X., Choy, W. Y., and Konermann, L. (2009) Solution-phase chelators for suppressing nonspecific protein-metal interactions in electrospray mass spectrometry. *Anal. Chem. 81*, 5008–5015.

66. Cannan, R. K., and Kibrik, A. (1938) Complex formation between carboxylic acids and divalent cations. *J. Am. Chem. Soc. 60*, 2314–2320.
67. Kebarle, P., and Verkerk, U. H. (2009) Electrospray: from ions in solutions to ions in the gas phase, what we know now. *Mass Spectrom. Rev. 28*, 898–917.
68. Schulz, D. M., Ihling, C., Clore, G. M., and Sinz, A. (2004) Mapping the topology and determination of a low-resolution three-dimensional structure of the calmodulin-melittin complex by chemical cross-linking and high-resolution FTICRMS: direct demonstration of multiple binding modes. *Biochemistry 43*, 4703–4715.
69. Kataoka, M., Head, J. F., Seaton, B. A., and Engelman, D. M. (1989) Melittin binding causes a large calcium-dependent conformational change in calmodulin. *Proc. Natl. Acad. Sci. U.S.A. 86*, 6944–6948.
70. Brokx, R. D., Lopez, M. M., Vogel, H. J., and Makhatadze, G. I. (2001) Energetics of target peptide binding by calmodulin reveals different modes of binding. *J. Biol. Chem. 276*, 14083–14091.
71. Konermann, L., Rosell, F. I., Mauk, A. G., and Douglas, D. J. (1997) Acid-induced denaturation of myoglobin studied by time-resolved electrospray ionization mass spectrometry. *Biochemistry 36*, 6448–6454.
72. Hu, J., Jia, X., Li, Q., Yang, X., and Wang, K. (2004) Binding of La^{3+} to calmodulin and its effects on the interaction between calmodulin and calmodulin binding peptide, polistes mastoparan. *Biochemistry 43*, 2688–2698.
73. Putkey, J. A., Ts'ui, K. F., Tanaka, T., Lagacé, L., Stein, J. P., Lai, E. C., and Means, A. R. (1983) Chicken calmodulin genes. A species comparison of cDNA sequences and isolation of a genomic clone. *J. Biol. Chem. 258*, 11864–11870.
74. Pan, J. X., Rintala-Dempsey, A., Li, Y., Shaw, G. S., and Konermann, L. (2006) Folding kinetics of the S100A11 protein dimer studied by time-resolved electrospray mass spectrometry and pulsed hydrogen-deuterium exchange. *Biochemistry 45*, 3005–3013.
75. Wilson, D. J., and Konermann, L. (2003) A capillary mixer with adjustable reaction chamber volume for millisecond time resolved studies by electrospray mass spectrometry. *Anal. Chem. 75*, 6408–6414.
76. Wang, G., and Cole, R. B. (1997) in Electrospray Ionization Mass Spectroscopy (Cole, R. B., Ed.) pp 137−174, John Wiley & Sons, Hoboken, NJ.
77. Konermann, L., and Douglas, D. J. (1998) Unfolding of proteins monitored by electrospray ionization mass spectrometry: a comparison of positive and negative ion modes. *J. Am. Soc. Mass Spectrom. 9*, 1248–1254.
78. Burger, D., Cox, J. A., Comte, M., and Stein, E. A. (1984) Sequential conformational changes in calmodulin upon binding of calcium. *Biochemistry 23*, 1966–1971.
79. Gau, B. C., Sharp, J. S., Rempel, D. L., and Gross, M. L. (2009) Fast photochemical oxidation of protein footprints faster than protein unfolding. *Anal. Chem. 81*, 6563–6571.
80. Tripathi, S., and Portman, J. J. (2009) Inherent flexibility determines the transition mechanisms of the EF-hands of calmodulin. *Proc. Natl. Acad. Sci. U.S.A. 106*, 2104–2109.
81. Kuprowski, M. C., and Konermann, L. (2007) Signal response of coexisting protein conformers in electrospray mass spectrometry. *Anal. Chem. 79*, 2499–2506.
82. Scaloni, A., Miraglia, N., Orrù, S., Amodeo, P., Motta, A., Marino, G., and Pucci, P. (1998) Topology of the calmodulin-melittin complex. *J. Mol. Biol. 277*, 945–958.
83. Llinás, R., Sugimori, M., and Silver, R. B. (1995) The concept of calcium concentration microdomains in synaptic transmission. *Neuropharmacology 34*, 1443–1451.
84. Zhao, M., Hollingworth, S., and Baylor, S. M. (1996) Properties of tri- and tetracarboxylate Ca^{2+} indicators in frog skeletal muscle fibers. *Biophys. J. 70*, 896–916.
85. Konermann, L., Pan, J., Simmons, D. A., and Wilson, D. J. (2007) in The Encyclopedia of Mass Spectrometry (Gross, M. L., and Caprioli, R. M., Eds.) pp 802−810, Elsevier, Amsterdam.
86. Alberty, R. A., and Silbey, R. J. (1996) Physical Chemistry, John Wiley & Sons, New York.
87. Kiefhaber, T., Quaas, R., Hahn, U., and Schmid, F. X. (1990) Folding of ribonuclease T1. 1. Existence of multiple unfolded states created by proline isomerisation. *Biochemistry 29*, 3053–3061.
88. Cheung, M. S., Klimov, D., and Thirumalai, D. (2005) Molecular crowding enhances native state stability and refolding rates of globular proteins. *Proc. Natl. Acad. Sci. U.S.A. 102*, 4753–4758.